Advanced Steel Construction – Vol. 20 No. 3 (2024) 253–265
DOI:10.18057/IJASC.2024.20.3.5

MECHANICAL PROPERTIES OF WEATHER-RESISTANT STEEL BEAM-TO-COLUMN CONNECTIONS

Yue-Dong Wang [1, 2], Ze-Yu Zhang[1, 4, *], Lu-Zhen Jiang [3], Li-Jing Zeng [1, 4] and Jie Liu [1, 4]

[1] *Central Research Institute of Building and Construction Co., Ltd., MCC Group, Beijing, 100088, China*
[2] *Tsinghua University, Beijing, 100084, China*
[3] *School of Civil Engineering, Hebei University of Science and Technology, Shijiazhuang, 050018, China*
[4] *National Engineering Research Centre For Steel Construction, Beijing, 100088, China*
** (Corresponding author: E-mail: 2008.zzy.good@163.com)*

ABSTRACT

Experimental research and numerical analysis are carried out on weather-resistant steel beam-to-column connections to investigate their mechanical properties in corrosive environment. Experiments of typical beam-to-column connections under normal condition and total corrosion condition are carried out respectively, and mechanical indexes such as failure mode, bearing capacity, deformation performance, and local plastic development of beam-to-column connections are compared and analyzed. Through collection and statistics of the monotonic tensile test data of weather-resistant steel, a calculation method of the constitutive relationship of weather-resistant steel under corrosion conditions is proposed. Accordingly, the numerical analysis of the weather-resistant steel beam-to-column connections is carried out. The results show that deformation and bearing capacities of weather-resistant steel beam-to-column connections decrease with the accumulation of corrosion-induced mass loss. The bearing capacity loss approximately changes in proportion to the corrosion mass loss (1:1), while deformation capacity loss of specimens (specifically referring to the ultimate displacement and ductility factor) is four times as much as the corrosion mass loss. In addition, the local corrosion of upper flange weld of the weather-resistant steel beam-to-column connection has the most significant effect on the deterioration of the mechanical properties of the connection. As the local corrosion zone is far away from the column, the deterioration effect of local corrosion on the beam upper and bottom flange tends to decrease.

ARTICLE HISTORY

Received: 17 July 2023
Revised: 21 February 2024
Accepted: 23 February 2024

KEYWORDS

Weather-resistant steel;
Beam-to-column connection;
Experimental research;
Numerical analysis;
Mechanical property

1. Introduction

Under the background of advocating green and low-carbon construction, developing high-performance steel structures has become an important part to help the low-carbon transformation of the construction industry and the construction of low-carbon cities. As a typical connection of high-performance steel structures, the investigation of the mechanical properties of weather-resistant steel beam-to-column connections holds significant theoretical and engineering importance.

Weather-resistant steel is based on ordinary steel by adding a small amount of Cu^0, Cr^{00}, Ni^{00}, Mo^0, and other alloying elements to form a dense and stable protective layer on the surface of steel matrix, so as to have excellent resistance of atmospheric corrosion. The corrosion resistance of weather-resistant steel can reach 2~8 times^0 that of ordinary steel, which can effectively mitigate the corrosion of steel structures. Collecting atmospheric exposure corrosion test data from typical test stations in China, Fig.1 shows the comparison of corrosion resistance performance between weather-resistant steel and ordinary steel. It can be seen that the corrosion resistance of weather-resistant steel is notably superior to that of ordinary steel. Especially with increase of corrosion time, this advantage becomes more and more obvious. In addition, weather-resistant steel not only has the recycling characteristics of ordinary steel but also can realize the application of coating free in actual engineering construction, which avoids the environmental pollution caused by spraying anti-corrosive coating. Based on the advantages mentioned above, weather-resistant steel has been popularized in some construction projects (see Fig.2) and has a very broad application prospect.

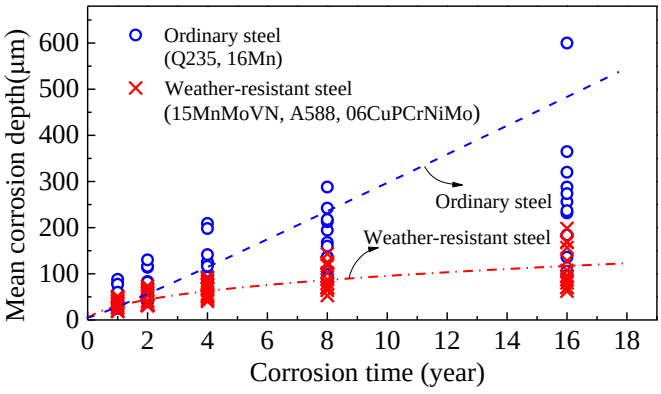

Fig. 1 Corrosion resistance performance of weather-resistant steel and ordinary steel

(a) Schematic diagram of National Sliding Centre

(b) Application area of weather-resistant steel

(c) Construction of weather-resistant steel frame

Fig. 2 Application example of weather-resistant steel in China——National Sliding Centre

At present, there have been some related studies on weather-resistant steel. FAN et al.^{0}, Chen W J et al.^{0}, and Gao et al.^{0} studied the corrosion behavior and morphology of corrosion products of ordinary carbon steel and weather-resistant steel in coastal atmospheric environment through cyclic dry-wet tests. They found that the corrosion rate of weather-resistant steel presents a trend of first fast and then slow, and the corrosion rate is lower than that of ordinary carbon steel. Zong et al.^{0} and Guo et al.^{0} studied the degradation law of monotonic tensile properties of weather-resistant steel after

corrosion and quantified the effect of corrosion mass loss on the deterioration of steel strength. Wu et al.[0] studied the mechanical properties of Q355 NHD weather-resistant rolled H-section steel component, and they proposed the partial coefficient of resistance and the design value of the strength for the corresponding component. Su et al.[0] and Zhang et al.[0] carried out high-cycle fatigue tests on weather-resistant steel after corrosion, and found that the corrosion pit could easily cause local stress concentration, which significantly reduced the fatigue resistance of weather-resistant steel. Hu et al.[0] and Albrecht et al.[0] studied the mechanical properties of welded joints of weather-resistant steel, and they found that the strength matching degree of base material and welding material and the pitting corrosion at the welding location would affect the corrosion resistance of welded joints of weather-resistant steel. Tao et al.[0] found that the roughness and treatment method of weather-resistant steel plate surface have a significant influence on the mechanical properties of bolted joints. In general, present researches on weather-resistant steel primarily centers on factors such as alloying element ratio, corrosion resistance of steel, and post-corrosion mechanical properties of steel components, etc. There are few researches on the connection of weather-resistant steel, which needs to be explored.

In this paper, experimental research and numerical analysis are carried out to investigate the mechanical properties such as failure mode, bearing capacity, and deformation capacity of weather-resistant steel beam-to-column connections in corrosive environment. The calculation method of material constitutive model of weather-resistant steel is proposed, and based on this, the influence law of corrosion mass loss and local corrosion location on the mechanical properties of weather-resistant steel beam-to-column connection is explored. The research of this paper is helpful to lay a foundation for improving the seismic design method of high-performance steel structures, which can give full play to the corrosion resistance of weather-resistant steel.

2. Experimental study

2.1. Specimen design

To explore mechanical properties of weather-resistant steel beam-to-column connections, specimens are designed and made. Fig. 3 shows configuration details of the specimen. The column of the specimen is steel tube with square section, and the sectional dimension $h\times b\times t$ is 200mm×200mm×14mm. The beam of the specimen has H section, and the sectional dimension $h\times b\times t_f\times t_w$ is 300mm×200mm×10mm×10mm. The beam is connected to column by a cantilever beam segment, and the cantilever beam segment is connected to the column by welding. The beam flange is connected with the cantilever beam segment by welding, and the beam web is connected with the cantilever beam segment by connecting plates and high-strength bolts. Stiffeners are arranged at the joint connection position in the column. Both ends of the column are fixed on the reaction frame to prevent sliding and out-of-plane deformation. The steel used in the specimens is weather-resistant steel Q355NH produced by Angang Group, and the bolts are high-strength grade 10.9 bolts (M24) made of weather-resistant steel. According to JGJ 82-2011, the test specimens are assembled and connected.

Two specimens are tested (named LZ-1 and LZ-2), and the difference is corrosion time. The corrosion time of LZ-1 is 0, and the corrosion time of LZ-2 is 360 hours. According to the "Corrosion tests in artificial atmospheres-Salt spray tests"(GB/T 10125-2021), specimen LZ-2 is corroded in Durability Laboratory at Tongji University. Fig. 4 shows the corrosion process of specimen LZ-2. After the specimen of weather-resistant steel beam-to-column connection is assembled, corrosion experiment is conducted in a specific corrosion environment. The corrosion solution used here is 5% NaCl salt solution, characterized by a pH range between 6.5 and 7.2. Fig. 5 shows the appearance of LZ-2 after corrosion. As shown in this figure, the corrosion products are attached to the specimen LZ-2, and the LZ-2 presents reddish brown in the whole body, which is global corrosion. Viewed from the naked eye, the distribution of the corrosion pit is relatively uniform, which shows the typical characteristics of corrosion for the weather-resistant steel.

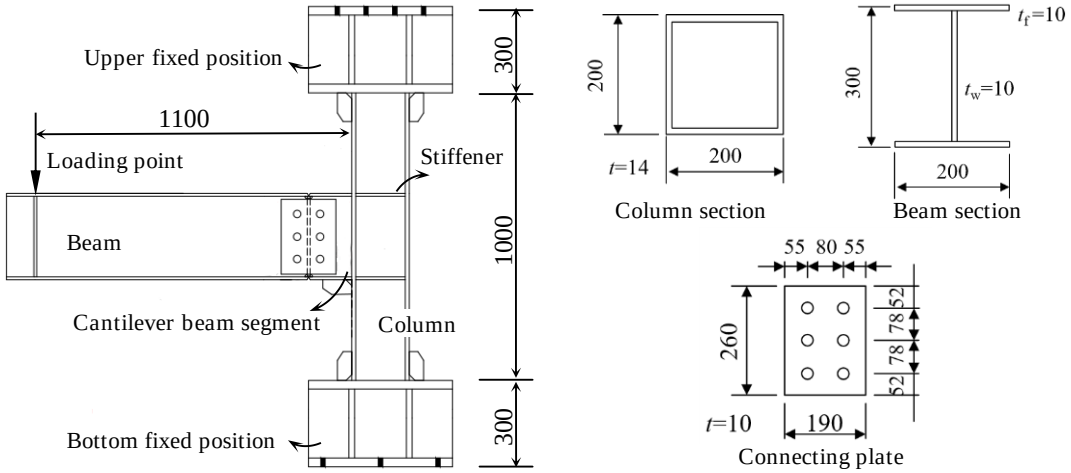

Fig. 3 Configuration details of the specimen (unit: mm)

(a)Corrosion test chamber (b)Specimen placement (c)Bolt hole protection (d)Corrosion completion

Fig. 4 Corrosion process of the specimen LZ-2

Fig. 5 LZ-2 appearance after corrosion

Fig.6 shows the arrangement of measuring points of the specimen. The displacement meters are used to measure the global deformation and the local deformation development is measured by strain gauges. The loading mode of LZ-1 and LZ-2 is the same. Both specimens carry out monotonic loading at the beam end, and the distance from the loading point to the column edge is 1100mm. When the specimen is unable to bear the load due to obvious failure or the beam end load drops to less than 85% of the peak load, the experiment is stopped.

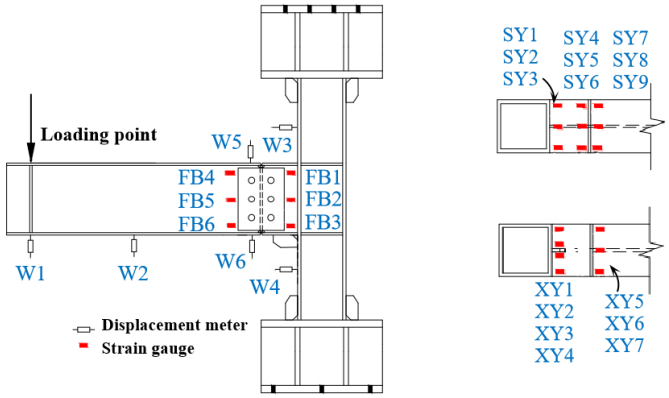

Fig. 6 Arrangement of measuring points of the specimen

2.2. Analysis of experimental results

2.2.1. Failure phenomenon

Fig.7 and Fig.8 show the failure phenomenon of LZ-1 and LZ-2, respectively. As shown in these figures, LZ-1 and LZ-2 have the same failure mode. With the increasing load, the beam-to-column connections are affected by the bending moment. The upper flange of beam is under tension, and the bottom flange of beam is under compression. The crack and final failure position of the specimen occurs on the beam's upper flange close to the edge of the column. The crack initiates at the position of flange end. Subsequently, the crack quickly penetrates along the through-thickness direction of the flange and expands towards to the beam web.

(a) Specimen installation

(b) Specimen damage

Fig. 7 Failure phenomenon of LZ-1

(a)Specimen installation

(b)Specimen damage

(c)Local damage

Fig. 8 Failure phenomenon of LZ-2

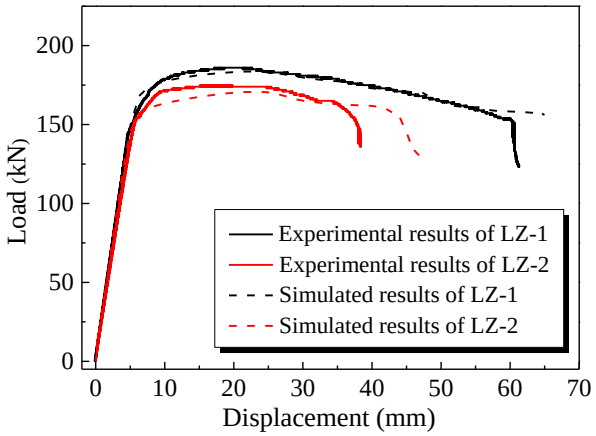

Fig. 9 Experimental and simulated Load-displacement curves

2.2.2. Load-displacement curve

Fig.9 illustrates load-displacement curves for LZ-1 and LZ-2 in the experiment. Firstly, the displacement increases linearly as the load increases. Subsequently, there exists an inflection point on the load-displacement curve, which indicates that the specimen has yielded. As displacement continues to increase, the specimen's load increases to the maximum, and peak load of LZ-1 and LZ-2 are 186kN and 175kN, respectively. Finally, large plastic deformation causes specimen's damage and cracking, leading to degradation of loading capacity. By comparing the two specimens' experimental load-displacement curves, it is evident that their curve forms are consistent. Under the influence of corrosion, compared with LZ-1, LZ-2's bearing capacity decreases by 6% and the deformation capacity decreases by 31.48%. Logically, for the weather-resistant steel beam-to-column connection under total corrosion, the negative effect of corrosion on the deformation is more significant, which should be paid attention to in practical construction.

2.2.3. Local deformation development

Fig. 10 shows the relationship between the strain gauge value and the specimen load, which represents the local strain development of the specimen. Throughout the loading process, the specimen's local plasticity mainly develops at beam flange, and the strain at beam web is generally in an elastic state (FB1~FB6). The beam upper flange is continuously under tension, and the strain values are all positive. The plastic development of beam upper flange near column (SY1, SY2, SY3) is the most significant. The beam bottom flange is continuously under compression, and the strain values are all negative. The plastic development of the beam bottom flange near the column (XY1, XY2, XY3, XY4) is significant, especially at the edge position of the flange (XY1 and XY4). The reason for the above result is that the edge position of the beam bottom flange is not constrained by the web and thus is prone to local buckling under compression, which leads to large plastic deformation at that position. In general, the local plastic development degree of LZ-2 is larger than that of LZ-1, due to the influence of corrosion.

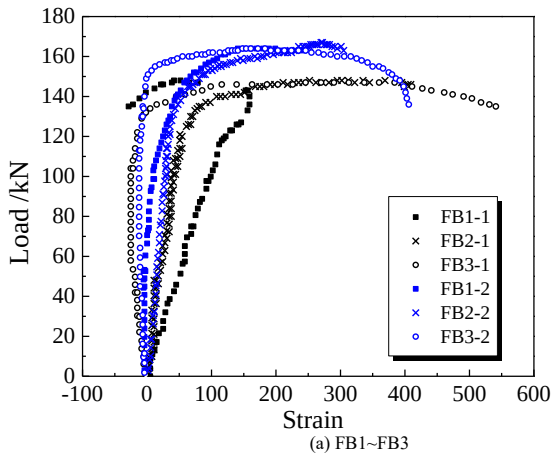

(a) FB1~FB3

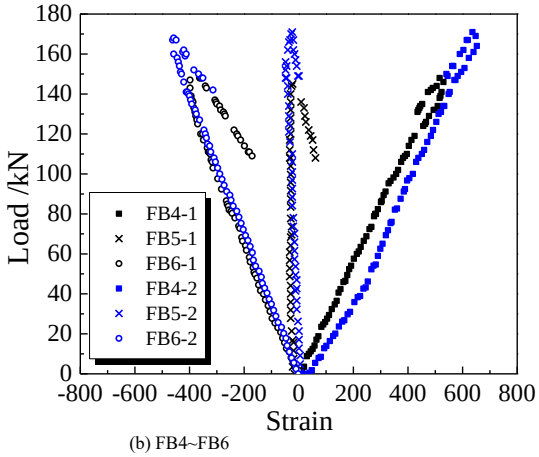

(b) FB4~FB6

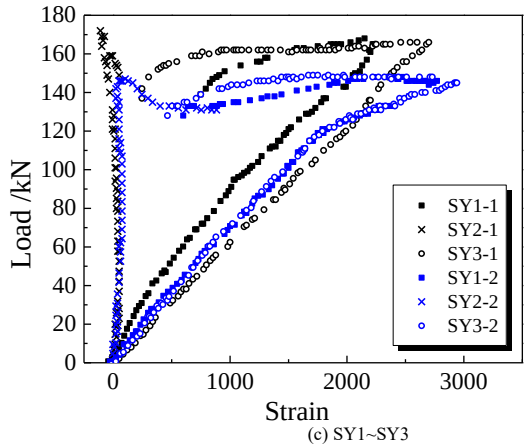

(c) SY1~SY3

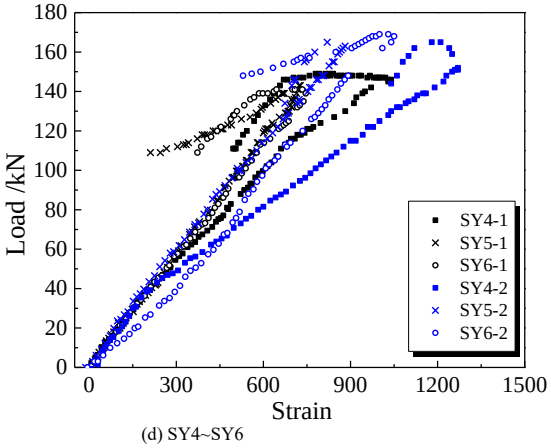

(d) SY4~SY6

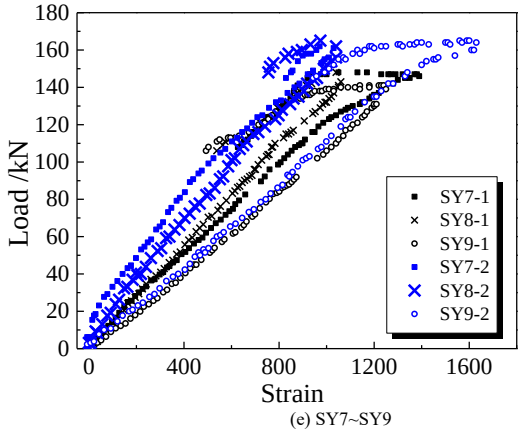

(e) SY7~SY9

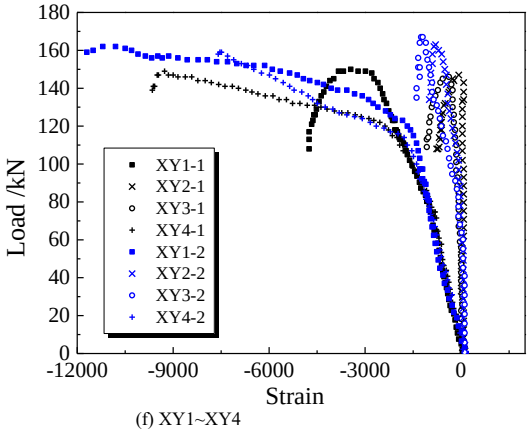

(f) XY1~XY4

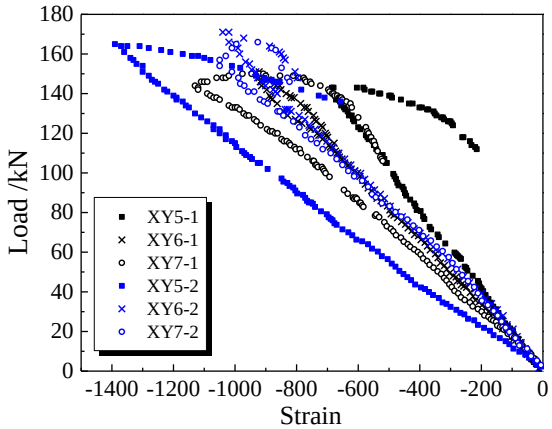

(g) XY5~XY7

Fig. 10 Local strain development (-1 represents LZ-1, and -2 represents LZ-2)

3. Numerical analysis

3.1. Finite element model

Fig.11 shows the specimen's finite element model utilized in ABAQUS platform. The specimen is simulated using solid element C3D8R. Considering calculation accuracy and efficiency, the key area of the specimen conducts mesh refinement. The simulation accurately replicates the practical experiment in terms of the specimen's actual size, boundary conditions, and loading mode. As shown in this figure, the fixed constraint is used as the boundary condition to simulate the constraint condition of column ends. Out-of-plane constraints are added in simulation to avoid the beam torsion. The "dumbbell" model is used to equivalent the actual high-strength bolt, and the preload is applied according to the actual test value. Considering the post-assembly interactions between components, friction coefficient of contact between bolt rod and bolt hole is 0.01, and the friction coefficient of contact between bolt cap and steel plate is 0.05. In addition, the cubic solid element is used to simulate the welding line, which is helpful to describe the mechanical behavior and failure state of beam-to-column connections.

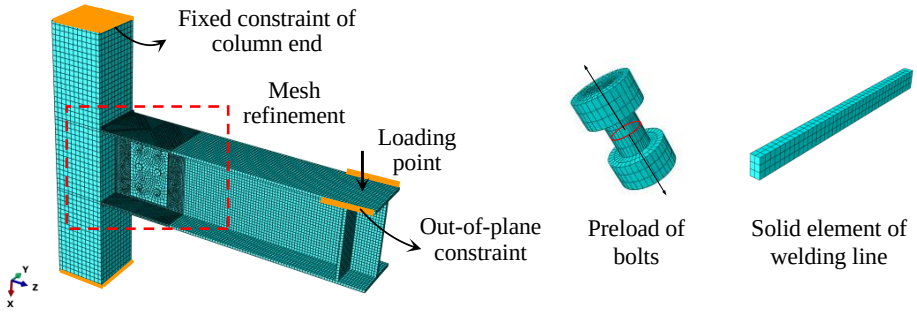

Fig. 11 Finite element model

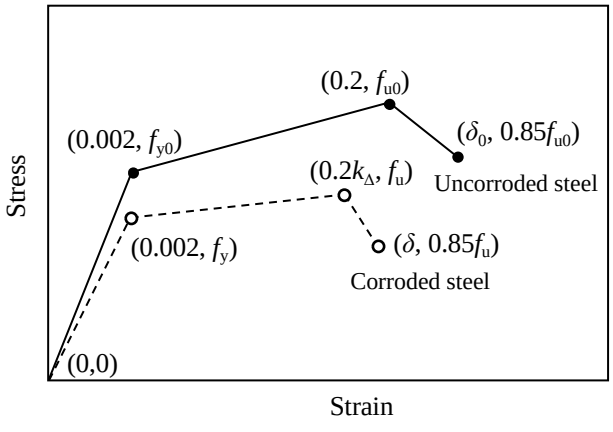

Fig. 12 Schematic diagram of weather-resistant steel constitutive model

3.2. Material model

To facilitate parametric analysis and mechanical property analysis of weather-resistant steel beam-to-column connections, a calculation method of the constitutive model of weather-resistant steel under different corrosion conditions is proposed. The proposed method transforms the complicated corrosion morphology modeling into a material physical model to approximately consider the corrosion's effect on mechanical properties of steel. In this calculation method, the trilinear model is used to describe the weather-resistant steel's stress-strain relationship under normal condition, and the stress-strain relationship of weather-resistant steel under corroded condition is formed by appropriate adjustment of this model. Fig. 12 shows the schematic diagram of weather-resistant steel constitutive model under normal and corroded conditions. In this figure, solid line represents the constitutive model of the uncorroded weather-resistant steel, which is determined by four coordinate points. Four coordinate points are (0, 0), (0.002, f_{y0}), (0.2, f_{u0}), and (δ_0, 0.85f_{u0}), respectively. Dash line represents the constitutive model of corroded weather-resistant steel, which is also determined by four coordinate points. Four coordinate points are (0, 0), (0.002, f_y), (0.2k_Δ, f_u), and (δ, 0.85f_u), respectively. f_{y0}, f_{u0} and δ_0 can be obtained by monotonic tensile test of weather-resistant steel under normal condition. Considering the time-consuming and high cost of corrosion tests, it is necessary to establish a relationship between mechanical properties of corroded steel and those under normal conditions, so as to obtain f_y, f_u and δ more conveniently and quickly.

Table 1 lists mechanical parameters of weather-resistant steel under normal and corrosive conditions. Sources of data include monotonic tensile tests of weather-resistant steel Q355NH[0], Q355NHD[0], Q345CNH[0], and HPS 485W[0]. To further quantify the corrosion's influence on mechanical properties of weather-resistant steel, data are normalized and corrosion reduction factors are introduced. The corrosion reduction factor of weather-resistant steel is determined by the ratio of the post-corrosion value of a mechanical parameter to the corresponding normal value of the mechanical parameter, which is shown as follows:

$$k_y = f_y / f_{y0} \tag{1}$$

$$k_u = f_u / f_{u0} \tag{2}$$

$$k = f_y f_{u0} / f_{y0} f_u \tag{3}$$

$$k_\Delta = \delta / \delta_0 \tag{4}$$

where k_y、k_u、k、k_Δ are corrosion reduction factors of steel yield strength, tensile strength, yielding-to-tensile ratio, and elongation, respectively. f_{y0} and f_y

are yield strength of weather-resistant steel under uncorroded and corroded conditions, respectively. f_{u0} and f_u are tensile strength of weather-resistant steel under uncorroded and corroded conditions, respectively. δ_0 and δ are elongation of weather-resistant steel under uncorroded and corroded conditions, respectively.

Table 1
Mechanical parameters of weather-resistant steel under normal and corrosive conditions

Steel type	Corrosion mass loss η(%)	Yield strength (MPa)	Tensile strength (MPa)	Yielding-to-tensile ratio	Elongation (%)
Q355NH	0	430.50	607.00	0.709	24.45
	1.501	419.33	594.00	0.706	23.68
	1.553	417.00	592.67	0.704	25.15
	1.867	404.33	580.33	0.697	24.62
Q355NHD	0	398.09	523.04	0.761	33.73
	5.203	375.70	515.09	0.729	23.77
	6.658	369.34	506.25	0.729	22.67
Q345CNH	0	588.53	859.6	0.685	/
	4.619	583.3	884.7	0.659	/
	4.500	534.8	834.3	0.641	/
	5.736	548.5	838.1	0.654	/
	5.806	547.8	829.4	0.660	/
	6.732	533.9	820.1	0.651	/
HPS 485W	0	578.9	858.4	0.674	/
	4.467	524.7	820.2	0.639	/
	6.154	537.4	829.5	0.648	/
	6.196	549.3	830.4	0.661	/
	6.601	526.1	827.9	0.635	/
	6.288	534.1	835.1	0.639	/

Considering the existing difference of corrosion environment in experiments of different types of weather-resistant steel, corrosion mass loss rather than corrosion time is used to quantify the corrosion degree of weather-resistant steel. According to experimental data, corrosion reduction factors and corrosion mass loss have a linearly negative relationship, which is shown as follows:

$$k_y = -1.094\eta + 1 \tag{5}$$

$$k_u = -0.4728\eta + 1 \tag{6}$$

$$k = -0.7323\eta + 1 \tag{7}$$

$$k_\Delta = -5.659\eta + 1 \tag{8}$$

Fig. 13 shows the expressions of corrosion reduction factors, which can be used to obtain and predict the constitutive model of weather-resistant steel under corrosion conditions. In the corrosion mass loss range of 0~7%, the corrosion-caused deterioration degrees on mechanical properties of steel from high to low are elongation, yield strength, yield-to-tensile ratio, and tensile strength. For example, at a corrosion mass loss of 0.07, the elongation, yield strength, yield-to-tensile ratio, and tensile strength of weather-resistant steel are 0.604, 0.923, 0.949, and 0.967 times of that of non-corroded steel, respectively. Due to the limitation of test data, the rule of performance degradation of other corrosion mass loss is worthy to be further studied.

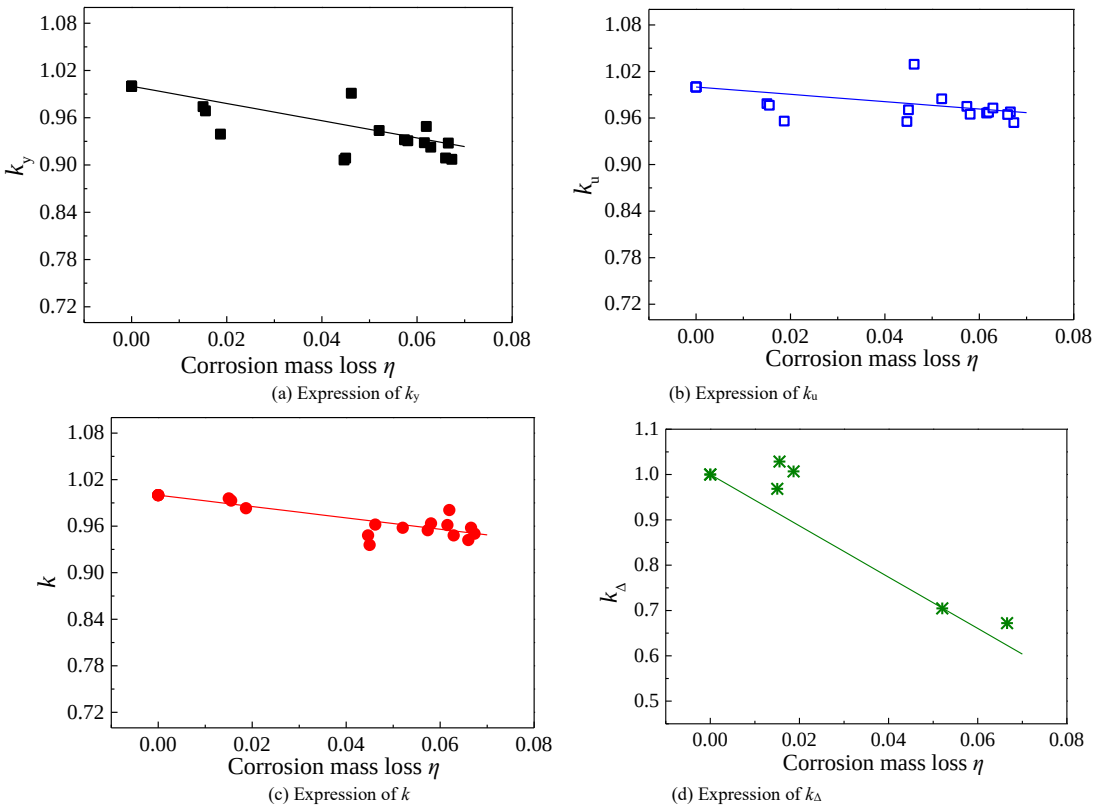

(a) Expression of k_y

(b) Expression of k_u

(c) Expression of k

(d) Expression of k_Δ

Fig. 13 Expressions of corrosion reduction factors of mechanical parameters

To describe the specimen's damage process, ductile damage model[0] is introduced to the material model in simulation, which is shown as follows:

$$\omega_D = \int_0^{\varepsilon_0^{pl}} \frac{d\varepsilon^{pl}}{\varepsilon_0^{pl}(T)} \tag{9}$$

$$T = \sigma_m / \sigma_e \tag{10}$$

$$\sigma_m = \frac{(\sigma_1 + \sigma_2 + \sigma_3)}{3} \tag{11}$$

$$\sigma_e = \sqrt{\frac{1}{2}\left[(\sigma_1 - \sigma_2)^2 + (\sigma_2 - \sigma_3)^2 + (\sigma_3 - \sigma_1)^2\right]} \tag{12}$$

where ε_0^{pl} is critical value of equivalent plastic strain. T is stress triaxiality, which can show the element's stress-state. ω_D is a state variable that monotonically increases with plastic deformation, serving as an indicator for the initiation of damage. σ_1, σ_2, and σ_3 are element's three principal stresses. σ_m and σ_e are mean stress and Mises equivalent stress, respectively. Damage initiation of the element in the simulated specimen occurs when the state variable accumulates to 1 throughout the loading history.

3.3. Simulated results

Fig.9 shows experimental and simulated load-displacement curves of LZ-1 and LZ-2. The experimental and simulated results exhibit similarity in several aspects, encompassing the curve shape, loading capacity, deformation performance, and capacity degradation. The error of loading capacity between experimental and simulated results is less than 4%. Fig.14 shows the local plasticity development of the specimen. As shown in this figure, the large value of Mises stress and plastic strain of the specimen is located in the beam upper flange close to the column, indicating that the local plasticity is mainly developed in that location. According to the stress triaxiality nephogram, the beam upper flange of the specimen is continuously under tension, while the beam bottom flange is continuously under compression. Some elements of the beam upper flange are under multi-directional tension state (T>1/3, and 1/3 represents that the element is under unidirectional tension). Based on damage initiation criterion[0], the critical value of equivalent plastic strain ε_0^{pl} is relatively small with the increase of the value of T (when T>1/3), and thus the damage is more prone to occur at the location where under multi-directional tension state. Fig.15 shows damage development of the specimen. The damage occurs at the beam upper flange end near the column, and the continuous accumulation of damage results in the cracking of the specimen. From these figures, we can see that the load-displacement curves, plasticity development, and the damage mode of experimental and simulated results are highly similar, showing a good accuracy of the finite element model. Therefore, the numerical simulation can effectively capture the mechanical performance of the weather-resistant steel beam-to-column connection, establishing a foundation for subsequent research on parameter analysis.

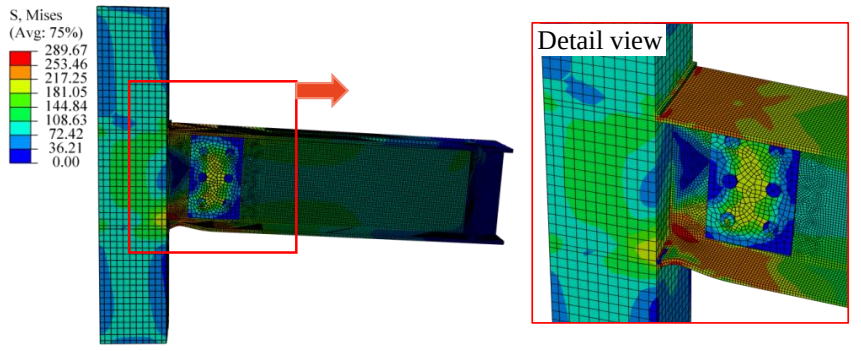

(a) Mises stress nephogram

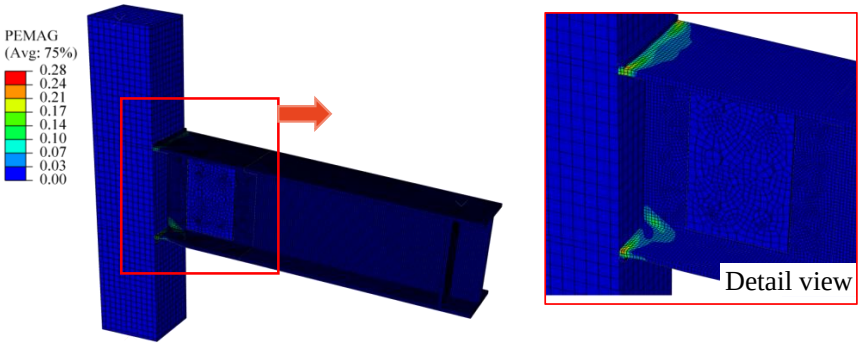

(b) Strain nephogram

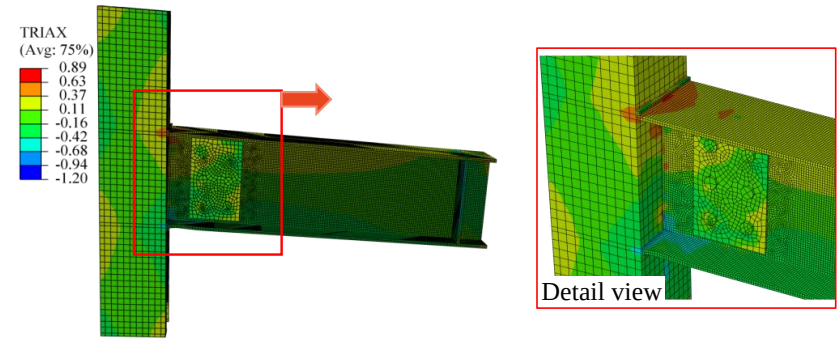

(c) Stress triaxiality nephogram

Fig. 14 Local plasticity development of the specimen

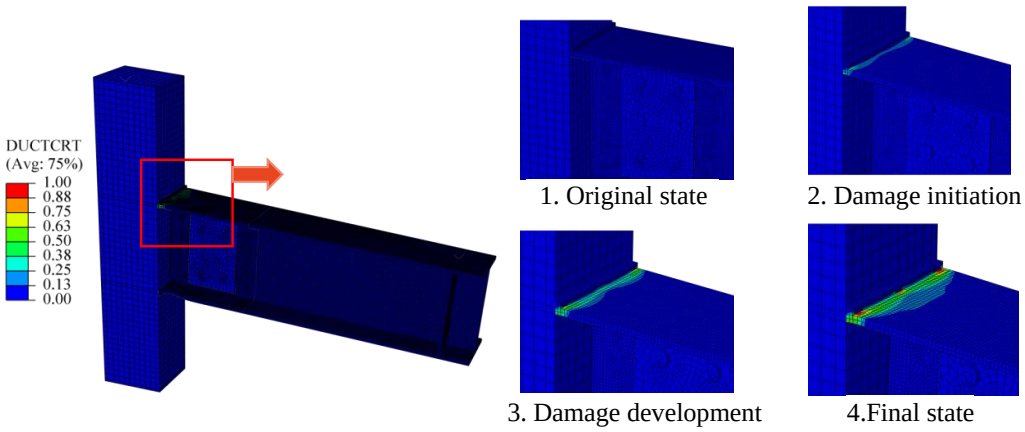

Fig. 15 Damage development of the specimen

4. Parametric analysis

4.1. Effect of corrosion degree

To further understand the influence regularity of corrosion on mechanical properties such as bearing capacity and deformation capacity of weather-resistant steel beam-to-column connections, corrosion mass loss is taken as variables (0, 0.01, 0.02, 0.03, 0.04, 0.05, 0.06, 0.07) to analyze the performance of specimens under total corrosion conditions. Fig. 16 shows specimens' simulated results of load-displacement curves under different corrosion mass losses. The shape of load-displacement curves of specimens is similar, which partly indicates that the failure modes of specimens under different corrosion mass losses are similar. As the corrosion mass loss increases, there is a tendency for the bearing capacity and deformation capacity of the specimen to decrease.

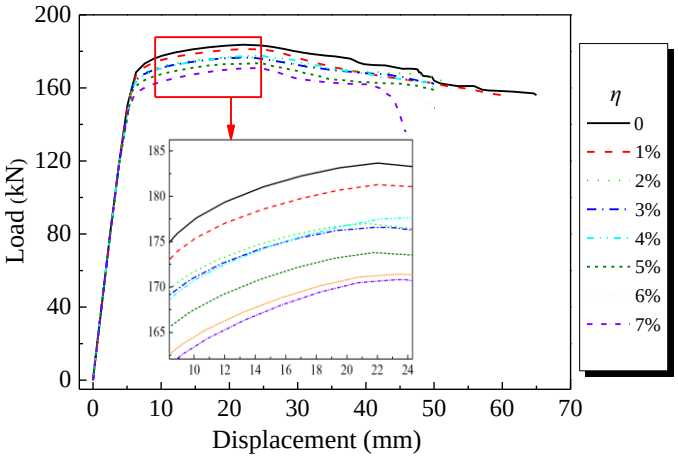

Fig. 16 Simulated results of load-displacement curves

Based on specimens' load-displacement curves, yield load F_y, peak load F_m, ultimate load F_u (85% of the peak load), and their corresponding displacements (including yield displacement Δ_y, peak displacement Δ_m, and ultimate displacement Δ_u) are obtained, as shown in Table 2. The ductility factor μ can be obtained by Δ_u/Δ_y. Fig. 17 shows the effect of corrosion degree on specimen loading capacity. It can be seen that the value of F_y, F_m, and F_u decrease with increase of corrosion mass loss which is in the range of 0~7%. Moreover, load loss rate of specimens exhibits a proportional variation with the corrosion mass loss, maintaining a 1:1 relationship. For example, the specimen with a corrosion mass loss of 7% will have a loading capacity loss of about 7% compared to that without corrosion. Fig. 18 shows the effect of corrosion degree on specimen deformation capacity. There is little change in Δ_y with the increasing corrosion mass loss, while Δ_m, Δ_u, and μ decrease with the increasing corrosion mass loss in the range of 0~7%. Moreover, the deformation capacity loss rate of specimens (specifically referring to Δ_u and μ) is four times as much as corrosion mass loss. For example, the specimen with a corrosion mass loss of 7% will have a deformation capacity loss of about 28% compared to that without corrosion.

Table 2
Mechanical parameters of weather-resistant steel beam-to-column connections

Corrosion mass loss η	Yield point		Peak point		Ultimate point		Ductility factor μ
	F_y/kN	Δ_y/mm	F_m/kN	Δ_m/mm	F_u/kN	Δ_u/mm	
0	168.60	6.32	183.68	22.02	155.56	64.55	10.21
1%	167.15	6.33	181.05	24.52	158.65	60.00	9.47
2%	160.76	5.70	177.02	21.35	162.51	52.58	9.22
3%	161.18	5.81	176.60	22.40	161.85	51.55	8.87
4%	159.16	5.69	177.69	24.75	160.00	50.05	8.79
5%	158.44	5.81	173.37	24.90	158.90	50.00	8.60
6%	157.44	6.00	171.40	23.26	148.98	48.85	8.14
7%	156.28	6.05	170.81	23.88	145.65	44.96	7.43

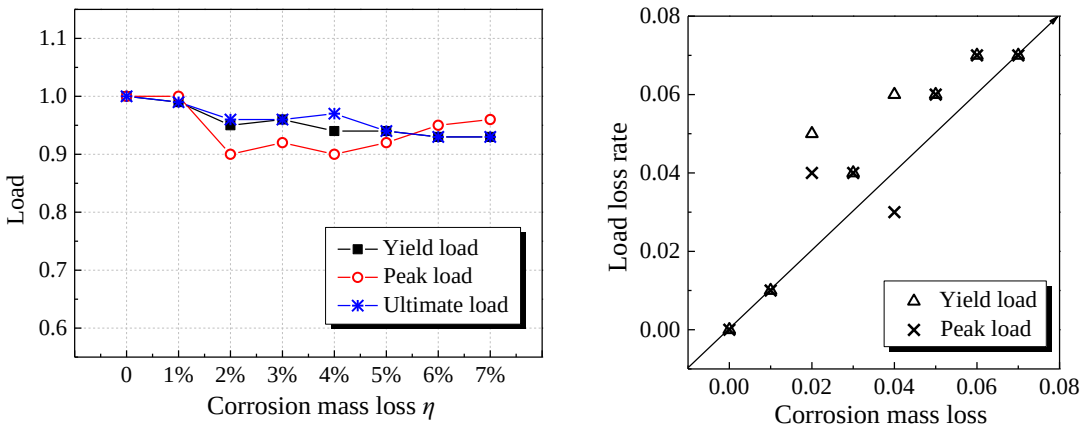

(a) Relationship of load and corrosion mass loss

(b) Relationship of load loss rate and corrosion mass loss

Fig. 17 Effect of corrosion degree on specimen loading capacity

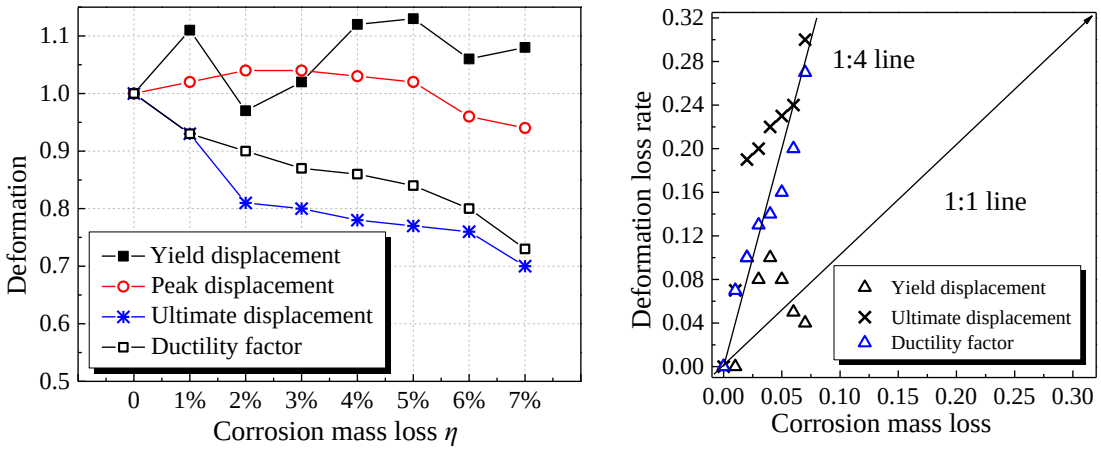

(a) Relationship of deformation and corrosion mass loss

(b) Relationship of deformation loss rate and corrosion mass loss

Fig. 18 Effect of corrosion degree on specimen deformation capacity

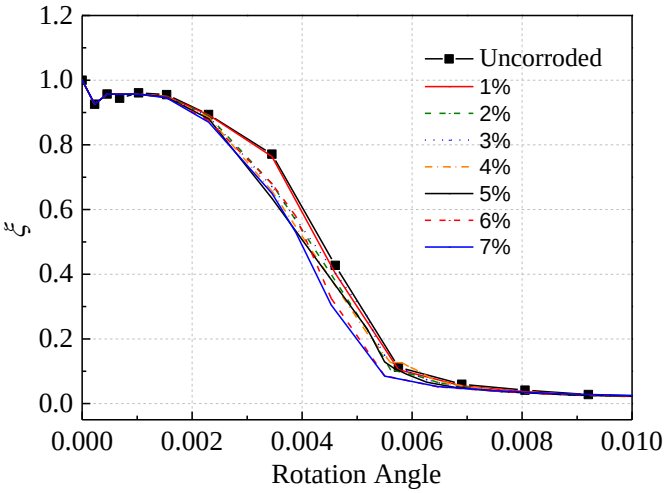

Fig. 19 Degradation of connection stiffness

To investigate the impact of corrosion degree on the connection stiffness of specimens, Fig. 19 shows the results of degradation of connection stiffness. ξ is the stiffness degradation coefficient, which is used to indicate the degree of stiffness degradation for the specimen. The calculation of this coefficient is Equation (13) and (14). The small value of ξ represents the large degradation.

$$K_i = \frac{\sum_{j=1}^{n} F_i^j}{\sum_{j=1}^{n} d_i^j} \tag{13}$$

$$\xi = \frac{K_i}{K_0} \tag{14}$$

where Ki is secant stiffness at the i-th level of loading, F_i^j is the peak force during the j-th cycle at i-th level of loading, and d_i^j is the horizontal displacement during the j-th cycle at the i-th level of loading. The specimen's secant stiffness decreases as the rotation angle increases. The reduction of ξ shows a slow-fast-slow trend. For beam-to-column connections with different corrosion degrees, their shape of stiffness degradation curves are approximately the same. In general, the large value of corrosion mass loss leads to relatively severe stiffness degradation.

4.2. Effect of local corrosion location

Due to different architectural forms and environmental conditions, apart from total corrosion, local corrosion is also a common type of corrosion in practical structures. Considering the randomness of local corrosion locations, the influence of local corrosion at different locations on mechanical properties of specimens is investigated. Local corrosion locations are W(see Fig.20), FS(see Fig.24), and FX(see Fig.28). W represents the location of welding line of beam and column, which includes W1(welding line of beam upper flange and column), W2(welding line of beam bottom flange and column), and W3(welding line of beam web and column). FS represents the local zone on the beam upper flange. Distance between the center of FS and the column end are 0.25*h*(*h* is the height of beam), 0.5*h*, 0.75*h*, 1.0*h*, 1.25*h*, 1.5*h*, 1.75*h*, and 2.0*h*, respectively, corresponding to FS025, FS050, FS075, FS100, FS125, FS150, FS175, and FS200. FX represents the local zone on the beam bottom flange. Distance between the center of FX and the column end are 0.25*h*(*h* is the height of beam), 0.5*h*, 0.75*h*, 1.0*h*, 1.25*h*, 1.5*h*, 1.75*h*, and 2.0*h*, respectively, corresponding to FX025, FX050, FX075, FX100, FX125, FX150, FX175, and FX200. The area of the local zone is 150mm×*b* (*b* is the width of beam). The constitutive relationship model of weather-resistant steel corresponding to the corrosion mass loss of 7% is taken as material properties of the local corrosion zone, and the numerical simulation analysis of specimens under different local corrosion conditions is carried out.

Fig. 21 shows the specimens' load-displacement curves in the condition of local corrosion of W. Local corrosion of W has a significantly negative effect on the mechanical performance of weather-resistant steel beam-to-column connection. Compared with total corrosion, local corrosion of W has limited influence on the bearing capacity of specimens, but more influence on the deformation of specimens. Fig. 22 shows the loading and deformation capacity of specimens in the condition of local corrosion of W. The local corrosion of W1 has the largest influence on the deterioration of mechanical properties of the specimen. With reference to non-corroded specimens, the local corrosion of W1 can lead to a 5% reduction in loading capacity and a 56% reduction in the deformation capacity of specimens, which should be paid significant attention to in practical engineering. Fig. 23 shows the connection stiffness of specimens in the condition of local corrosion of W. The local corrosion of W1 has the relatively large negative influence on the specimen's rotational stiffness.

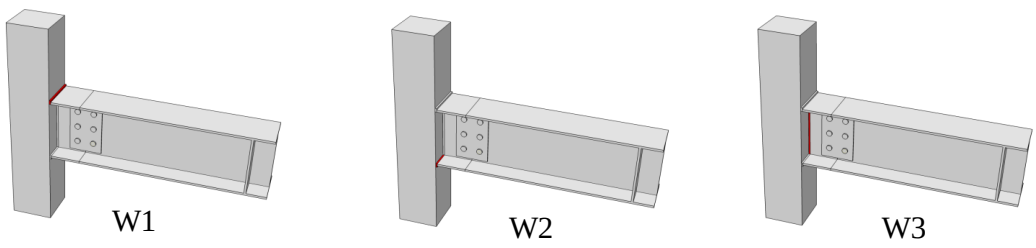

Fig. 20 Schematic diagram of local corrosion location of W (red represents corrosion)

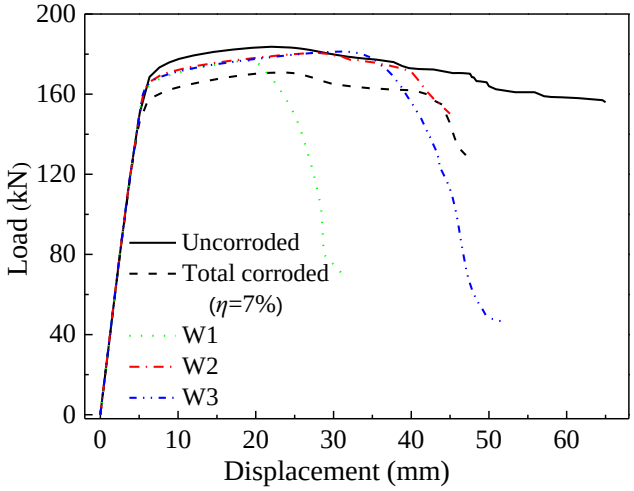

Fig. 21 Load-displacement curves of local corrosion of W

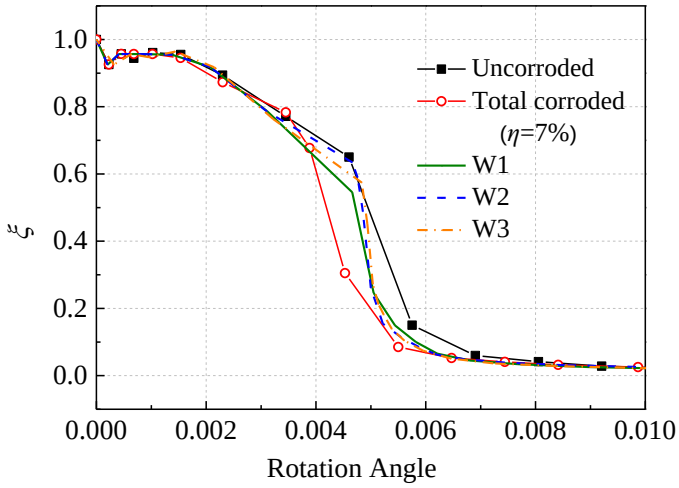

Fig. 23 Connection stiffness of local corrosion of W

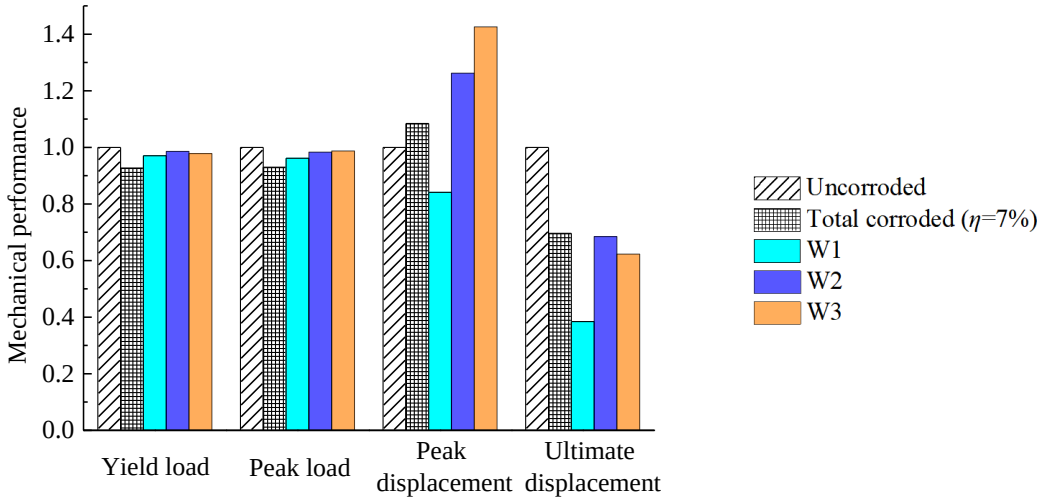

Fig. 22 Loading and deformation capacity of local corrosion of W

Fig. 25 and Fig. 29 show the specimens' load-displacement curves in the condition of local corrosion of FS and FX, respectively. Fig. 26 and Fig. 30 show the load capacity of specimens in the condition of local corrosion of FS and FX, respectively. In these figures, local corrosion of FS and FX both have a similarly negative effect on the bearing performance of weather-resistant steel beam-to-column connection. Under the condition of local corrosion of FS, the deterioration effect on the bearing capacity comes from tensile damage of steel. Under the condition of local corrosion of FX, the deterioration effect on the bearing capacity comes from the likely local buckling of steel plate. When the distance between the center of local corrosion zone (FS or FX) and the column end is 0.25~0.75 times the beam height, the deterioration effect of local corrosion on the bearing capacity is relatively more significant, which is related to the plastic hinge length at the beam end of the beam-column connection (generally 0.5 times the beam height). Moreover, the closer distance between center of the local corrosion zone and column end, the more significant effect of local corrosion on the deterioration of bearing capacity. For example, for specimens of FS025 and FX025, the bearing capacity decreases by about 4%. When the distance between the center of the local corrosion zone (FS or FX) and column end is larger than 1.25 times the beam height, there will be no effect on the mechanical behavior of the specimen.

Fig. 27 and Fig. 31 show the connection stiffness of specimens in the condition of local corrosion of FS and FX, respectively. In these figures, local corrosion of FS and FX both have a similarly negative effect on the stiffness degradation of weather-resistant steel beam-to-column connection. The deterioration effect of FS corrosion on the rotational stiffness comes from the tensile damage of beam's upper flange, while the the deterioration effect of FX corrosion on the rotational stiffness comes from the likely local buckling of beam's bottom flange. In general, the near distance between the center of local corrosion zone (FS or FX) and the column end results in the relatively severe stiffness degradation.

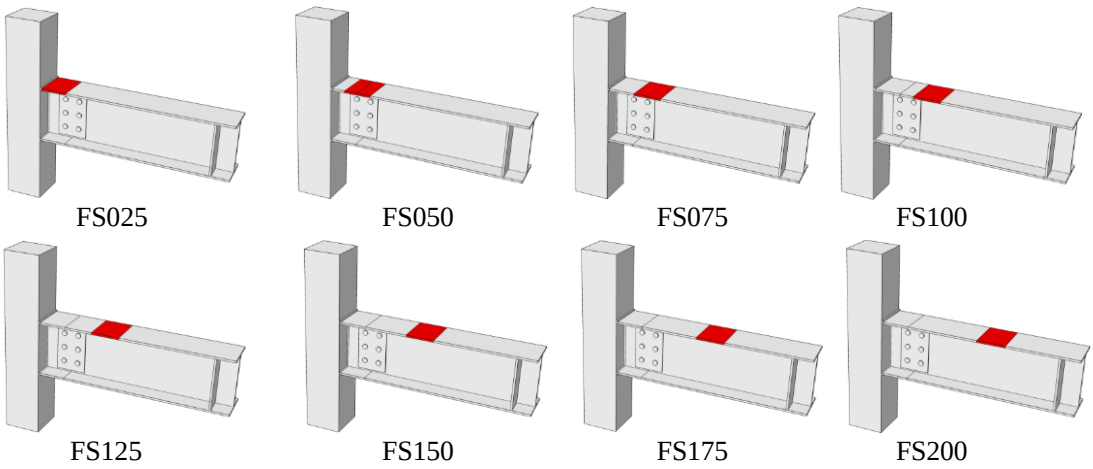

Fig. 24 Schematic diagram of local corrosion location of FS (red represents corrosion)

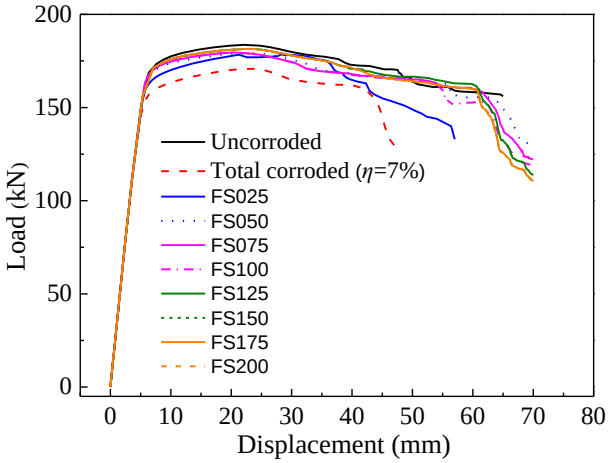

Fig. 25 Load-displacement curves of local corrosion of FS

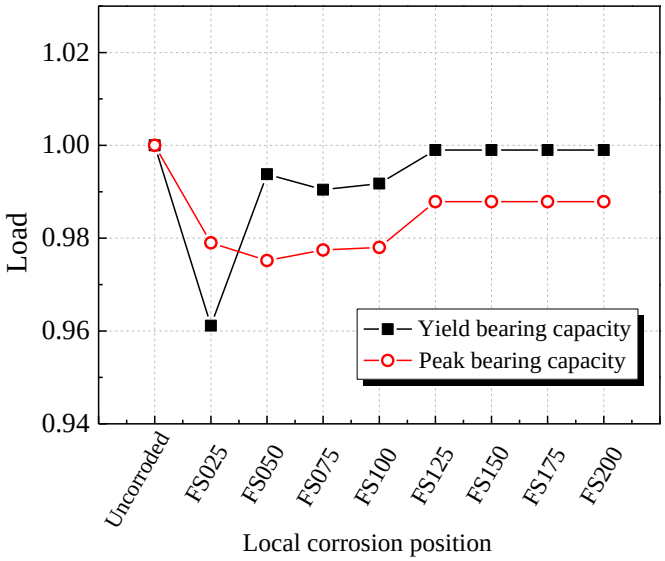

Fig. 26 Load capacity of local corrosion of FS

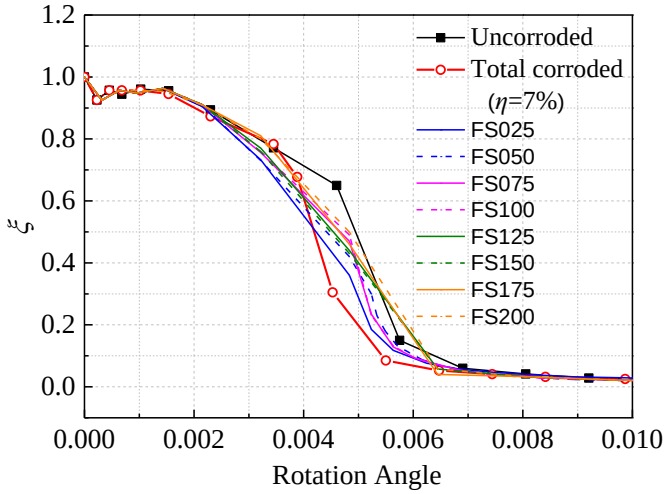

Fig. 27 Connection stiffness of local corrosion of FS

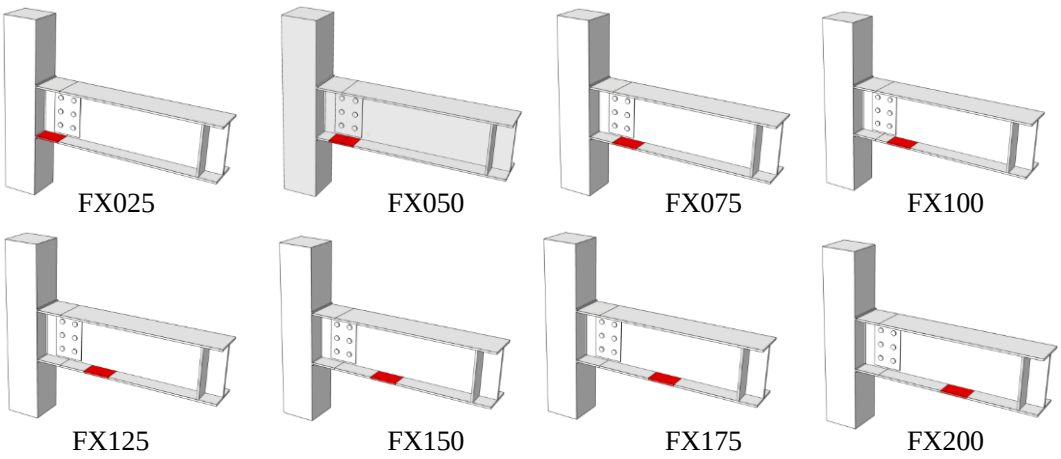

Fig. 28 Schematic diagram of local corrosion location of FX (red represents corrosion)

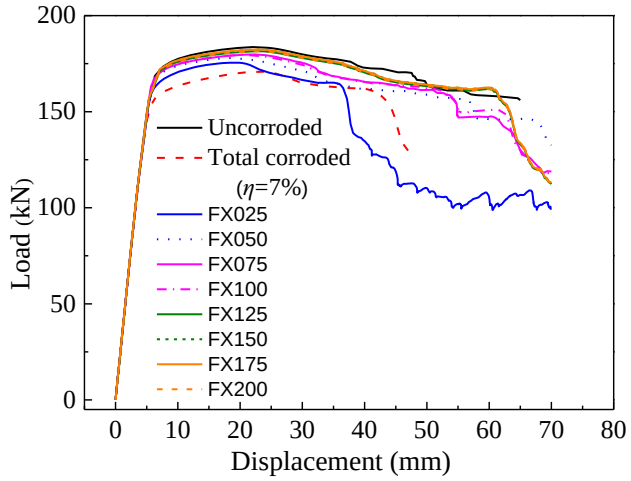

Fig. 29 Load-displacement curves of local corrosion of FX

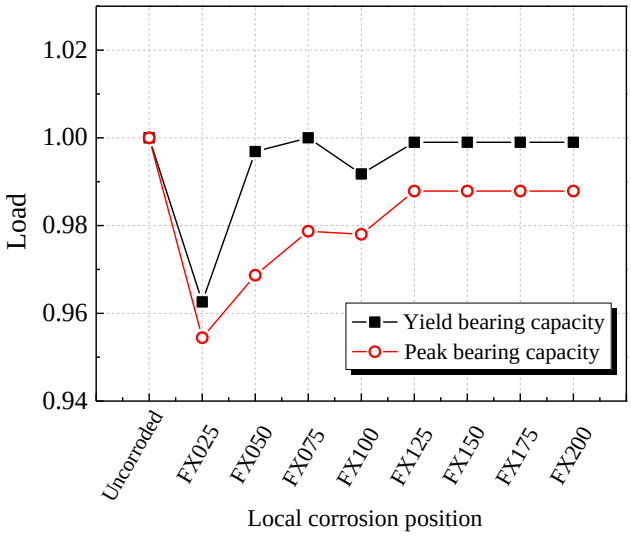

Fig. 30 Load capacity of local corrosion of FX

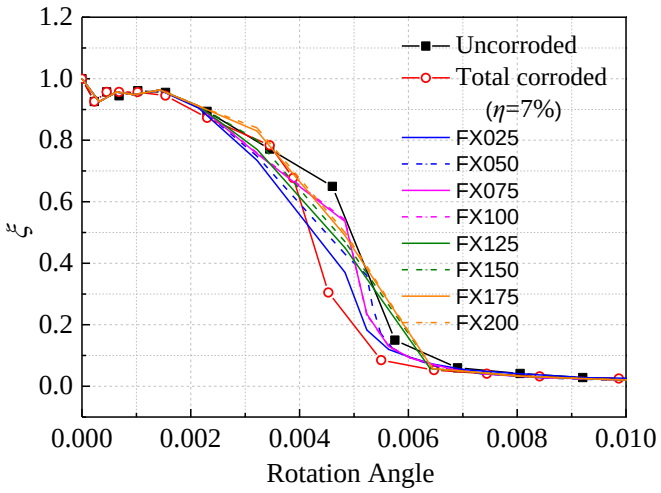

Fig. 31 Connection stiffness of local corrosion of FX

5. Conclusions

Experiments and numerical analysis are carried out on weather-resistant steel beam-to-column connections to investigate the mechanical properties in the corrosive environment. The main findings and conclusions are summarized as follows:

(1) Experimental results show that the weather-resistant steel beam-to-column connection under condition of total corrosion has similar failure mode and plasticity development of the connection under the normal condition. The local plasticity and initial cracking of the specimen mainly develop on beam's upper flange near column end, and the beam web is in an elastic state. Under the same loading condition, the plastic development degree of specimens after total corrosion is higher than that of specimens without corrosion.

(2) Mechanical parameters of weather-resistant steel (including yield strength, tensile strength, yield-to-tensile ratio, and elongation) have a linearly negative relationship with corrosion mass loss. Accordingly, a calculation method of the constitutive model of weather-resistant steel under different corrosion conditions is proposed. Using this method, the mechanical performance and damage development can be truly described.

(3) Under the condition of total corrosion, the bearing capacity, deformation capacity and connection stiffness of weather-resistant steel beam-to-column connections decrease with the increase of corrosion mass loss in the range of 0~7%. The bearing capacity loss of specimens is approximately in the same proportion as the corrosion mass loss (1:1), while the deformation capacity loss of specimens (specifically referring to the ultimate displacement and ductility factor) is four times as much as corrosion mass loss.

(4) The local corrosion of W1 of the weather-resistant steel beam-to-column connection has the most significant effect on the deterioration of the mechanical properties of the connection. With reference to non-corroded specimens, the local corrosion of W1 can lead to 56% reduction in deformation capacity of specimens, which should be paid significant attention to in practical engineering.

(5) When the distance between the center of local corrosion zone (FS or FX) and the column end is 0.25~0.75 times the beam height, the deterioration effect of local corrosion on the bearing capacity is relatively more significant, and closer distance results in more deterioration of bearing capacity. When the distance between the center of the local corrosion zone (FS or FX) and the column end is larger than 1.25 times the beam height, there will be no effect of local corrosion on the mechanical behavior of the specimen.

Acknowledgments

The authors gratefully acknowledge the financial support from the Jining City Global ranking project (2022JBZP004) and the Science and Technology Planning Project of the Ministry of Housing and Urban-Rural Development of the People's Republic of China (2022-K-145).

References

[1] Zhang T, Liu W, Chen L, et al. On how the corrosion behavior and the functions of Cu, Ni and Mo of the weathering steel in environments with different NaCl concentrations[J]. Corrosion Science, 2021, 192: 109851.
[2] YANG X, YANG Y,et al. A new understanding of the effect of Cr on the corrosion resistance evolution of weathering steel based on big data technology[J]. Journal of Materials Science and Technology, 2022, 104: 67.
[3] SUN M, DU C, LIU Z, et al. Fundamental understanding on the effect of Cr on corrosion resistance of weathering steel in simulated tropical marine atmosphere[J]. Corrosion Science, 2021, 186: 109427.
[4] Jia J, Liu Z, Cheng X, et al. Development and optimization of Ni-advanced weathering steel: A review[J]. Corrosion Communications, 2021, 2: 82-90.
[5] CHENG X Q, JIN Z, LIU M, et al. Optimizing the nickel content in weathering steels to enhance their corrosion resistance in acidic atmospheres[J]. Corrosion Science, 2017,115:135.
[6] XIAO X M, PENG Y, MA CY, et al. Effects of alloy element and microstructure on corrosion resistant property of deposited metals of weathering steel[J]. International Journal of Iron and Steel Research, 2016, 23(2): 171.
[7] Shi Yongjiu, Yu Xianglin, Ban Huiyong, et al. Research and application on high performance structural steel and its structural system[J]. Building Structure, 2021,51(17):145-151.
[8] FAN Y, LIU W, et al. Evolution of rust layers on carbon steel and weathering steel in high humidity and heat marine atmospheric corrosion[J]. Journal of Materials Science and Technology, 2020, 39: 190.
[9] Chen W J, Hao L, Dong J H, et al. Effect of sulphur dioxide on the corrosion of a low alloy steel in simulated coastal industrial atmosphere[J].Corrosion Science, 2014, 83(7): 155-163.
[10] Gao Xiuhua, Cheng Yujun, Sun Chao, et al. Study on anti-corrosion properties of extra-weathering steel Q350EWR1[J]. Materials Science and Technology, 2019, 27(3):9.
[11] Zong Liang, Zhang Juzheng, Zhao Bo, et al. Study on the mechanical properties of weathering steel Q355NHD after corrosion in an industrial marine atmospheric environment[J]. China Journal of Highway and Transport, 2022, 35(06):168-179.
[12] Guo X Y, Kang J F, Zhu J S, et al. Corrosion behavior and mechanical property degradation of weathering steel in marine atmosphere[J]. Journal of Materials in Civil Engineering, 2019, 31(9): 04019181.
[13] Wu Yaohua, He Wenhui, Wang Houxin. Research on properties and design strength values of weather resistance rolled h-shape steel[J]. Steel Construction, 2019, 34(02):20-30.
[14] Su Han, Zhao Liguo, et al. Study On Fatigue Behavior of Corroded Butt Welded Joints Made of Weathering Steel Q345qDNH[J]. Journal of Building Structures, 2021,42(S2):473-481.
[15] ZHANG Y, ZHENG K, ZHU J, et al. Research on corrosion and fatigue performance of weathering steel and high-performance steel for bridges[J]. Construction and Building Materials, 2021, 289: 123108.
[16] Hu Jie, Huang Cui, He Yaling, et al. Influence of The Match between Weathering Steel Metal and Welding Wire on Stress Corrosion Resistance of Welded Joints[J].Corrosion & Protection, 2018, 39(06):425-430.
[17] Albrecht P, Lenwari A. Fatigue strength of weathered A588 steel beams[J] Journal of Bridge Engineering, 2009, 14(6): 436-443.
[18] Tao Xiaoyan, Shi Zhiqiang, Han Jiyue, et al. Experimental research on high strength bolted

connection of weathering steel bridge[J]. Steel Construction, 2018, 33(01):105-108.
[19] CHEN Y Y, TZEBG H J, WEIB L I, et al. Corrosion resistance and mechanical properties of low-alloy steels under atmospheric conditions[J].Corrosion Science, 2005, 47:1001-1021.
[20] Zhang Lele. Study on corrosion resistance and mechanical properties of weathering steel after corrosion[D]. Hebei University of Science and Technology, 2020.
[21] Zong Liang, Zhang Juzheng, Zhao Bo, Zhang Fujun. Study on the mechanical properties of weathering steel Q355NHD after corrosion in an industrial marine atmospheric environment[J]. China Journal of Highway and Transport, 2022, 35(06):168-179.
[22] Zhang Yu. Research on corrosion fatigue properties of weathering steel and high performance steel[D]. Southwest Jiaotong University, 2020.
[23] Zeng L, Zhang W, Li H. Low-cycle fatigue life prediction of I-shaped steel brace components and braced frames[J]. Thin-Walled Structures, 2021, 163: 107711.